Minimum-Fuel, Three-Dimensional Flight Paths for Jet Transports

Frank Neuman*
NASA Ames Research Center, Moffett Field, California
and
Eliezer Kreindler†
Israel Institute of Technology, Haifa, Israel

Representative minimum-fuel flight paths of various types are computed for a commercial jet transport, particularly in the terminal area, and used to evaluate near-optimal approximations for onboard, on-line application. The aircraft is modeled by point-mass equations constrained by equilibrium of vertical forces; the three-dimensional position, heading, and speed are the five state variables, and the bank angle, thrust, and flight-path angle are the three controls. Relatively long flight paths (over 5 n.mi.) from an arbitrary initial state to a fixed final state are computed. These flight paths have center segments that are nearly straight in their horizontal projections, with altitude variations consistent with earlier work, which used a simple energy state model. The computed paths, however, extend the earlier work to three dimensions and include the turning climb-out and descent portions, which must be present for flight paths between distant, unaligned runways. The effect on fuel consumption of the FAA-imposed limit of 250 knots indicated airspeed is also examined.

I. Introduction

THE many publications dealing with flight-path optimization can be classified according to the type of aircraft and mission, the performance index, and the modeling complexity. Recent studies of fuel minimization concentrate on flight in a vertical plane (e.g., Refs. 1-6). A few works have appeared on three-dimensional flight (e.g., Refs. 7-11), but only Ref. 11 is on flight by commercial jet transports. The latter paper treated only the climb-out and descent portions of complete long-range flight paths below 10,000 ft altitude.

The work reported herein on three-dimensional fight paths extends that of Ref. 12 on horizontal flights by adding altitude as a state variable and flight-path angle as a control variable. We study only relatively long flight paths (over 5 n.mi.) that have a nearly straight center segment on the horizontal x-y plane projection and that may have turns at either or both ends. The short (2-5 n.mi.), highly turning paths, explored in Ref. 12 for horizontal flight, are not included because they entail small altitude changes, their occurrence is rare, they are hard to approximate, they are prone to Darboux points,[13,14] and their fuel consumption is low.

In complete three-dimensional flight paths, the aircraft is to reach a desired state (three-dimensional position, heading, or velocity) from some arbitrary initial state. Such flight paths occur between airports whose runways have different headings where the initial state would be the departure point and the desired state would be at the approach-initiation point. They also may arise in the descent phase when the aircraft does not arrive in the terminal area at the proper state in preparation for landing (e.g., for air-traffic control reasons). In this paper we will consider flight paths that begin and end at the same altitude, which are representative of paths between airports. Furthermore, we will concentrate on flight paths in the range of 5-50 n. mi., since they display all the features of a complete flight path and they fit our aircraft model, which is valid only up to an altitude of 10,000 ft. To overcome this limitation, we also developed a special performance index that permitted us to study the low-altitude (up to 10,000 ft) portions of long flight paths, and we show that these portions are compatible with the solutions for the long flight paths described in published reports.[1] Special cases of flight paths that we considered were those confined to a vertical plane[15]; we refer to these as *nonturning* flight paths, in contrast to three-dimensional ones with turns.

The objective of this work was to discover the common characteristics of representative families of optimal flight paths in order to identify those characteristics that provide the most fuel savings. This is essential in order to devise near-optimal algorithms that can eventually be implemented on board in real time. A corollary objective was the fuel-consumption comparison of such near-optimal flight paths with the optimal ones. We also wanted to find the extent to which the optimal flight paths violate the FAA-imposed 250 n.mi. indicated airspeed (IAS) constraint and the extra fuel needed for meeting this constraint optimally.

The optimal flight paths were obtained by computing extremals, namely, paths that satisfy the necessary conditions of the minimum principle. This involves the numerical solution of the state and costate differential equations from appropriate initial values. The selection of the initial costate variables is greatly faciltated by the fact that on each flight path the flight-path angle is for the most part a singular control. This method is not suitable for onboard application. The method given in Ref. 1, however, is suitable and it may be combined near optimally with our results to include initial and final turns.

In this paper, the problem statement in Sec II is followed by three sections of analytical results: computing the necessary conditions, the singular flight-path angle, and the speed constraint (Secs. III, IV, and V, respectively). The computations of the extremals is outlined in Sec. VI, followed by numerical results for climb-outs and descents (Sec. VII) and for complete three-dimensional flight paths (Sec. VIII). These results are discussed in Sec. IX. Numerical values for the fuel flow rate and drag functions, and formulas for the singular flight-path angle are in Appendices A and B, respectively.

Received Aug. 24, 1984; revision received Feb. 1, 1985. This paper is declared a work of the U.S. Government and therefore is in the public domain.

*Research Scientist.
†Associate Professor, Department of Electrical Engineering.

II. Problem Statement

The point-mass equations of motion we employ are

$$\dot{x} = v\cos\psi \tag{1}$$

$$\dot{y} = v\sin\psi \tag{2}$$

$$\dot{h} = v\gamma \tag{3}$$

$$\dot{\psi} = -gu/v \tag{4}$$

$$\dot{v} = g(T-D-W\gamma)/W \tag{5}$$

These equations are derived by assuming 1) a small angle of attack adjusted so that lift = weight/cosϕ, 2) a small flight-path angle γ, 3) coordinated turns, 4) no winds, and 5) a constant weight (see, e.g., Ref. 15). Here x and y are the coordinates in the horizontal plane, h is the altitude, ψ a ground-track angle measured counterclockwise from the x axis, v the true airspeed, g the gravitational constant, and W the weight. For simplicity, winds were not considered. They were considered in Ref. 1 as $v_n(h,x,y,t)$, which presents the practical solution for the straight-line portion of the flight paths. We considered the weight to be a constant 150,000 lb. This is justified, since the actual weight change caused by fuel consumption over the longest flight path considered here is only 0.025%. (For further discussion for weight change, see Ref. 16.)

The first of three controls is the thrust T, constrained by $T_{\text{idle}} \le T \le T_{\max}$. Technically, both T_{idle} and $T_{\max}$ are h and v dependent. However, the idle thrust is small enough to be negligible, and, for simplicity, the maximal thrust was chosen as $T_{\max} = 23{,}000$ lb, the smallest maximal value allowable over the altitude range of 0-10,000 ft. The second control is the tangent u of the bank angle ϕ. It is positive with the right wing down and constrained by $|\phi| \le |\phi_m|$ where $\phi_m = 30$ deg, the currently used passenger-comfort limit in commercial autopilots. The third control is the flight-path angle γ; since it appears linearly, it must be constrained by $\gamma_{\min} \le \gamma \le \gamma_{\max}$ when it is not singular. We make the somewhat arbitrary, but representative, choice of $\gamma_{\max} = 5$ deg to prevent deceleration during climb at maximum thrust and $\gamma_{\min} = -4$ deg to prevent acceleration during descent at idling thrust; increasing the range of allowable γ to allow for such deceleration and acceleration will not materially change the numerical results. Initial and final altitudes are chosen to be 2000 ft to allow for obstacle clearance and glide-slope alignment for climb-out and descent, respectively; the initial and final speeds are chosen to be typical of the initial climb and the final approach and landing speeds of the modeled commercial jet aircraft. In the optimization, dips below 2000 ft occurred. To prevent such dips, we at times changed the limits to $\gamma_{\min} = 0$ deg for climb-out and $\gamma_{\max} = 0$ deg for descent.

On some flight paths we imposed the FAA limit of 250 knots (422 ft/s) on the indicated airspeed v_I. In terms of the true airspeed v, this is a state variable inequality constraint,

$$S(v,h) = c - v_I(1+qh) \le 0; \quad v_I = 422 \text{ ft/s},$$
$$q = 1.62\times 10^{-5} \text{ ft}^{-1} \tag{6}$$

For our altitude range of 2000-10,000 ft, Eq. (6) represents a true airspeed limitation of 258-291 knots.

The drag, including flap deployment at low speeds, is modeled by

$$D(h,v,u) = D_1(h,v) + D_2(h,v)u^2 \tag{7}$$

where flaps are deployed continuously such that the drag is minimized for a given altitude and speed, a certain angle of attack is not exceeded ($\alpha \le 8$ deg), and the fuel flow rate by

$$F(h,v,T) = C_0(h,v) + C_1(h,v)T + C_2(h,v)T^2 \tag{8}$$

The functions D and F are polynomial least-square fits to tabular numerical values. Numerical values are for a Boeing 727 type of jet transport in the terminal area. Details and numerical values are provided in Appendix A and Ref. 16.

The objective is to minimize the fuel consumption

$$J = \int_0^{t_f} F(h,v,T)\,dt \tag{9}$$

over a flight path; here t_f is open. Problems with a predetermined t_f are called four-dimensional problems and are considerably more complicated. This is the appropriate performance index for complete flights that include both climb-out and descent. Since our drag and fuel-flow models were limited to an altitude of 10,000 ft, we did not compute complete long-range flights that include a high-altitude cruise portion. However, one can take into account the cruise portion for climb-outs and descents as follows.

The down range of flight is at $\psi = 0$, in the direction of the x axis. Thus, a turn during a climb-out or descent contributes the distance $\int v\cos\psi dt$ along the x axis. If C is the fuel per nautical mile expended at optimal cruise speed and altitude (see Ref. 1), then $C\int v\cos\psi dt$ can be thought of as the fuel saving that a climb-out or descent contributes to the overall flight by shortening the cruise section. Thus, for climb-out and descent, one should use the index

$$J' = \int_0^{t_f} [F(h,v,T) - Cv\cos\psi]\,dt \tag{10}$$

It is shown in the next section, however, that the aim of the performance index [Eq. (10)], which is to study the low-altitude portions of long three-dimensional flight paths, can equivalently be achieved by the use of the index [Eq. (9)] together with an appropriate choice of costate values. In other words, the climb-out and descent portions for long flight paths are special cases of the complete three-dimensional flight paths.

III. Necessary Conditions

We consider first the minimizaiton of J as defined in Eq. (9). According to the minimum principle (e.g., Ref. 17), the Hamiltonian is given by

$$H = \lambda_0 F(h,v,T) + \lambda_x v\cos\psi + \lambda_y v\sin\psi + \lambda_h v\gamma - \lambda_\psi gu/v$$
$$+ \lambda_v g[T - D(h,v,u) - W\gamma]/W + \eta[v - v_I(1+qh)] \tag{11}$$

where $\lambda_0 \ge 1$; since solutions with $\lambda_0 = 0$ will not be considered, we henceforth set $\lambda_0 = 1$. Here, the λ's are the costate variables to the corresponding state variables; F and D are given by Eqs. (8) and (7), respectively; and η is the multiplier for the speed constraint [Eq. (6)] satisfying[18]

$$\eta(t) \le 0, \qquad \eta(t)S[v(t),h(t)] \equiv 0 \tag{12}$$

The costate variables are given by

$$\dot{\lambda}_x = -H_x = 0 \rightarrow \lambda_x = \text{const} \tag{13}$$

$$\dot{\lambda}_y = -H_y = 0 \rightarrow \lambda_y = \text{const} \tag{14}$$

$$\dot{\lambda}_h = -H_h = -F_h + \lambda_v g D_h/W + \eta v_I q \tag{15}$$

$$\dot{\lambda}_\psi = -H_\psi = \lambda_x v\sin\psi - \lambda_y v\cos\psi \tag{16}$$

$$\dot{\lambda}_v = -H_v = -F_v - \lambda_x \cos\psi - \lambda_y \sin\psi$$
$$-\lambda_h \gamma - \lambda_\psi g u/v^2 + \lambda_v g D_v/W - \eta \tag{17}$$

where $H_x = \partial H/\partial x$, etc. Since the final time t_f is free and $H_t = 0$, we have the condition, for optimal control, of

$$H = 0 \quad \text{all} \quad t\epsilon(0, t_f) \tag{18}$$

Minimization of H with respect to T and u is identical to that in Ref. 12 and it yields

$$\begin{aligned} T^* &= T_{\max} && \text{if} \quad \tau \geq T_{\max} \\ &= \tau && \text{if} \quad T_{\text{idle}} < \tau < T_{\max} \\ &= T_{\text{idle}} && \text{if} \quad \tau \leq T_{\text{idle}} \end{aligned} \tag{19}$$

where

$$\tau = -[C_1(h,v) + \lambda_v g/W]/[2C_2(h,v)] \tag{20}$$

and

$$\begin{aligned} u^* &= \mu && \text{if} \quad |\mu| < u_m \quad \text{and} \quad \lambda_v < 0 \\ &= u_m \operatorname{sgn}\lambda_\psi && \text{if} \quad |\mu| \geq u_m \quad \text{and} \quad \lambda_v < 0 \\ &= u_m \operatorname{sgn}\lambda_\psi && \text{if} \quad \lambda_v \geq 0 \quad \text{and} \quad \lambda_\psi \not\equiv 0 \end{aligned} \tag{21}$$

where

$$\mu = -W\lambda_\psi/[2v\lambda_v D_2(h,v)] \tag{22}$$

If $\lambda_v > 0$ and $\lambda_\psi \equiv 0$ on an interval, then minimization of H with respect to u calls for $u = \pm u_m$. But this is incompatible with Eqs. (14) and (16), which, together with the fact that λ_x and λ_y are constant, imply that $u \equiv 0$ if $\lambda_\psi = 0$. This can be resolved by allowing a "chattering" (or "relaxed") $u(t)$, which chatters at infinite frequency equally between $+u_m$ and $-u_m$. We note from Eq. (20) that $\tau < 0$ when $\lambda_v > 0$ and hence $T = T_{\text{idle}}$. Thus, a chattering $u(t)$ may be called for in the case of certain end states that require a nonturning flight, $T = T_{\text{idle}}$, and maximum drag for deceleration. If a chattering u is not allowed, then the optimal solution does not exist between these end states, but will exist for neighboring end states. We note that allowing a chattering $u(t)$ makes the originally nonconvex velocity set convex (see Appendix C of Ref. 16).

Minimization of H with respect to γ yields at once

$$\begin{aligned} \gamma^* &= \gamma_{\max} && \text{if} \quad H_\gamma < 0 \\ &= \gamma_{\min} && \text{if} \quad H_\gamma > 0 \\ &= \gamma_{\min} \leq \gamma \leq_{\max} && \text{if} \quad H_\gamma = 0 \end{aligned} \tag{23}$$

where

$$H_\gamma = \lambda_h v - \lambda_v g \tag{24}$$

Clearly, γ^* can assume intermediate values only if $H_\gamma \equiv 0$ on an interval. These values are termed *singular* in the theory of optimal control; portions of an optimal solution with a singular control are called *singular arcs*. The case of singular γ is treated in the next section. The switching of γ is, of course, unrealistic, but it is an acceptable price to pay for a simplified model where γ is a control rather than a state variable.

So far we have considered complete three-dimensional flight paths. For climb-out and descent portions of long flight paths, we replace the performance index [Eq. (9)] by Eq. (10). Furthermore, for Eq. (10) the terminal coordinates x and y are free, since we are interested in merging the cruise segment as opposed to attaining a specific point in space, and hence by the transversality condition $\lambda_x = \lambda_y = 0$. We observe that both changes can be effected by using the original index [Eq. (9)] and setting in the Hamiltonian of Eq. (11)

$$\lambda_x = -C, \qquad \lambda_y = 0 \tag{25}$$

and, therefore, we need to develop only one set of necessary conditions. Here, we recall, C is the fuel consumed per nautical mile when crusing at the optimal altitude and speed; among other factors such as the cruise weight, it depends on the length of the cruise portion. In our numerical work, $C = 17.5$ lb/n.mi., which from Ref. 1 is for a 200 n.mi. flight.

Ignoring the term $-Cv\cos\psi$ in Eq. (10) or, equivalently, setting $C = 0$ in the performance index is incorrect. For example, compare two speed-constrained climb-outs, both to 10,000 ft with a 68 deg heading change. The first, minimizing the performance index [Eq. (10)], requires 1258 lb of fuel. The second, minimizing Eq. (9), requires 7 lb less fuel; however, its range is 2.93 n.mi. shorter, which will cost an additional 51 lb of fuel along the cruise portion. Thus, when considering the overall flight, the climb-out for which the term $-Cv\cos\psi$ in Eq. (9) is ignored requires 3.5% more fuel than the one that does not.

IV. Singular Flight-Path Angle

We assume in this section that the speed constraint is inactive, i.e., $\eta = 0$ in Eq. (11). Along the singular arc H_γ, the coefficient of γ in the Hamiltonian (11), given by Eq. (24), is identically zero. Hence

$$\lambda_h = g\lambda_v/v \tag{26}$$

Furthermore, all time derivaties of H_γ must vanish. This is used to evaluate the singular γ. In our case, γ appears explicitly (and linearly) in $\ddot{H}_\gamma$. Using $0 = H = H_\gamma = \dot{H}_\gamma = \ddot{H}_\gamma$ yields the form

$$A + B\gamma = 0 \tag{27}$$

where A and B are lengthy functions (see Appendix B) of nearly all state, costate, and control variables (save γ, of course). The generalized Legendre-Clebsch condition,[19] here $(-\ddot{H}_\gamma)_\gamma = B \geq 0$, is checked numerically while computing

$$\gamma = -A/B \tag{28}$$

and is found to be satisfied strongly in all computed cases. We remark that Eq. (28) contains $\dot{T}$ and $\dot{u}$ (the latter via $\dot{D}$), which causes discontinuities in the singular γ when the thrust or the bank angle reach their limits.

The nonturning case, $\gamma = \psi = \lambda_y = \lambda_\psi = u = 0$, $D = D_l$, is worth special attention. Then, Eqs. (18) and (26) give (see also Ref. 15)

$$\lambda_v = -W(F + \lambda_x v)/[g(T - D_l)] \tag{29}$$

Equation (29) with the conditions $H_\gamma = \dot{H}_\gamma = 0$ gives

$$\lambda_v = W(Fg/v - F_h v - F_v g)/[g(D_{l_h} v - D_{l_v} g)] \tag{30}$$

and

$$\lambda_x = -F/V - \lambda_v g(T - D_l)/(vW) \tag{31}$$

Equating (29) with (30) and recalling that F and D, and their partial derivatives, depend on h and v, give a function

$$G(h, v, T, \lambda_x) = 0 \tag{32}$$

The use of the above equations for the numerical computation is commented upon in Sec. VI. For climb-out and descent of long flight paths, it turns out in all numerical solutions that on the singular arc the thrust is maximal and idle, respectively. Further, since $\lambda_x = -C$, Eq. (32) is thus an implicit function of h and v and it gives the v-h profile for a nonturning climbout or descent without having to compute the singular $\gamma(t)$. In fact, having the v-h profiles for either a complete flight path or the climb-out or descent of a long flight path we can compute γ as follows. Dividing Eq. (3) by Eq. (5) we have

$$h' \triangleq \mathrm{d}h/\mathrm{d}v = v\gamma/[g(T-D)/W - g\gamma)]$$

whence

$$\gamma = (T-D)h'/[W(v/g+h')] \tag{33}$$

where $h' \cong \Delta h/\Delta v$ is numerically computed from Eq. (32). For turning flight paths $D = D(v,h,u)$, the dependence on u makes use of Eq. (33) impractical and Eq. (28) is used for the numerical calculations. Another disadvantage of Eq. (33) is that it has no Legendre-Clebsch condition to check for optimality.

For complete three-dimensional flight paths, the method of finding the v-h profile and then γ from Eq. (33) is complicated by the fact that, on the central part of the singular arc, T is intermediate (see Ref. 16 for details). As a check, we used both Eqs. (28) and (33) for computing the v-h profiles and singular γ for nonturning climb-out, descent, and complete three-dimensional flight paths and obtained the same results.

V. The Speed Constraint

When the speed constraint [Eq. (6)] is active, then

$$v(t) = v_I[1 + qh(t)] \tag{34}$$

Differentiating Eq. (34) and substituting Eqs. (3) and (5) for $\dot{h}$ and $\dot{v}$, respectively, and solving for γ gives

$$\gamma = [g(T-D)/W]/[g + v_I^2 q(1+qh)] \tag{35}$$

It turns out that γ given by Eq. (35) is intermediate, its coefficient in the Hamiltonian is $H_\gamma \equiv 0$, and it is thus singular. For convenience of designation, we call "singular arc" those parts of a flight path for which γ is singular and the speed constraint is either inactive or is not being obeyed; when the speed constraint is active we refer to a "speed-constraint arc" even though γ is singular.

At a junction time t_i of singular and speed-constraint arcs, $\gamma(t)$ is discontinuous. It is shown in Ref. 16 that the costates λ_h and λ_v, affected by the speed constraint, are continuous across the junction. This agrees with the necessary conditions given in Ref. 20, which were derived, however, for a scalar control.

The condition $\eta(t) \geq 0$ must be checked along the speed-constraint arc. Furthermore, $\eta(t)$ is needed for the computation of λ_v and λ_h. To compute the multiplier η, we differentiate Eq. (26), substitute for v and $\dot{v}$ from Eq. (34) and for $\dot{h}$, $\dot{\lambda}_h$, and $\dot{\lambda}_v$ from their respective differential equations. This yields η, and thus

$$\eta = [C_{0_h} + C_{1_h}T + C_{2_h}T^2 - \lambda_v g D_h/W - g(vA_\eta + \lambda_v \dot{v})/v^2]/(v_I q + g/v) \geq 0 \quad \text{on the constraint} \tag{36a}$$

$$\eta = 0 \quad \text{off the constraint} \tag{36b}$$

where

$$A_\eta \triangleq C_{0_v} + C_{1_v}T + C_{2_v}T^2 - C\cos\psi + \lambda_h\gamma + \lambda_\psi g u/v^2 - \lambda_v g D_v/W \tag{37}$$

VI. Remarks on the Computation of Extremals

As stated in the introduction, we obtain our example results by computing extremals. An extremal is computed by forward and backward integration of the state and costate equations (1-5) and (12-16), respectively, with the controls given by Eqs. (19-24), starting at a point of known or assumed state and costate variables. However, unless care is exercised, most of such extremals will provide flight paths of little interest. If an extremal contains arcs for which special relationships between state an costate variables must hold (such as singular or state-constraint arcs), that is where numerical computation must start. These relationships are helpful because they limit the search for initial values of the state and costate variables.

Computations of climb-out and descent extremals start at time t_s at $h(t_s) = h_s = 10{,}000$ ft. There γ is singular and u is practically zero; thus, $v(t_s)$ is determined by Eq. (32) with $\lambda_x = -C$, giving $v(t_s) = v_s = 331$ knots for climb-outs and $v_s = 275$ knots for descents. On climb-outs, the speed constraint of 250 knots IAS is violated; if we choose to observe it, $v = 290$ knots at $h = 10{,}000$ ft. The starting values of the state and costate variables are thus $x_s = y_s = \psi_s = \lambda_y = \lambda_\psi(t_s) = 0$, $h_s = 10{,}000$ ft, $v(t_s) = v_s$, $\lambda_x = -C$, and $\lambda_h(t_s)$ and $\lambda_v(t_s)$ are determined by Eqs. (26) and (29), respectively. Thus, for nonturning extremals, all states and costates at the starting time t_s are determined and so is the singular arc of the climb-out and descent. For turning extremals, it suffices to take very small $\lambda_\psi(t_s) \neq 0$ to produce the turns shown in Fig. 1.

For complete three-dimensional flight paths, $h(t_s)$ is to be chosen. Since T is intermediate around the peak altitude passing continuously from $T_{\max}$ to $T = 0$ (see Fig. 2b below) and u is practically zero there, a convenient starting value is $T(t_s) = D_I$ (which is not the $\gamma = 0$ point; see Fig. 2a). Thus, for nonturning extremals, $v(t_s)$ is determined by Eq. (32), $\lambda_v(t_s)$ by Eq. (30), $\lambda_h(t_s)$ by Eq. (26), and the constant λ_x in Eq. (31) is $\lambda_x = -F/v$. The remaining starting state and costate variables $(x,y,\lambda_y,\lambda_\psi)$ are set to zero. We store values of $(x,h,v,\lambda_h,\lambda_v,T,\gamma)$ on nonturning extremals to serve as starting points for turning extremals for which $\lambda_y \neq 0$. The choice of the starting point and the magnitude and sign of λ_y are used to obtain the desired turns at the ends of the extremals.

VII. Results: Climb-out and Descent Flight Paths

Analytically, climb-outs and descents are only portions of complete paths. The former, being simpler, will be discussed first.

Figures 1a and 1b show climb-out flight paths from 2000 ft and 180 knots to 10,000 ft. We observe that:

1) There is an initial descent at $\gamma = \gamma_{\min} = -4$ deg, during which most of the turn and most of the acceleration take place with relatively little altitude drops.

2) The actual climb is for the most part nonturning at an almost constant singular flight-path angle of $\gamma \cong 4.4$.

3) The singular-arc climb is essentially decoupled from the amounts of initial turn and the v-h profile is practically independent of them.

4) Figure 1b shows that large turns start with the maximum bank angle of $\phi_m = 30$ deg.

5) Although not shown in Fig. 1b, the result is that the thrust is $T = T_{\max}$ throughout, including the initial turn.

For descents, the thrust is $T = T_{\text{idle}} = 0$ throughout. The descents are therefore far less fuel critical than the climb-outs, but their characteristics are very similar to those listed above for the climb-outs. Descents are shown in Fig. 1c; for large turns we observe a surprising final switch from $\gamma = \gamma_{\max} = 5$ deg to $\gamma = \gamma_{\min} = -4$ deg.

As stated earlier, the dips during the turn portions of climb-outs and descents below 2000 ft might be unacceptable. Entirely level turns were secured by imposing the *ad hoc* constraints $0 \leq \gamma \leq 5$ deg and $-0.01 \leq \gamma \leq 0$ deg *only during the*

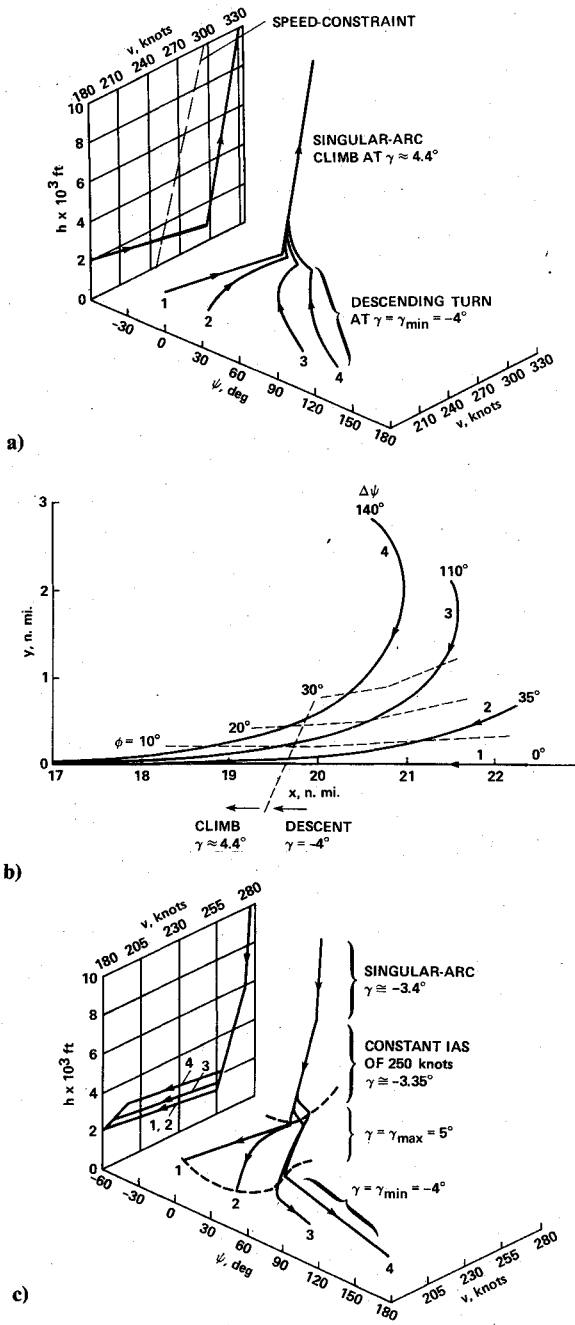

Fig. 1 Climb-out and descent paths: a) climb-out trajectories in (h,ψ,v) space with no speed constraint; b) x-y plot of turns for climb-out; c) descent trajectories in (h,ψ,v) space with speed constraint.

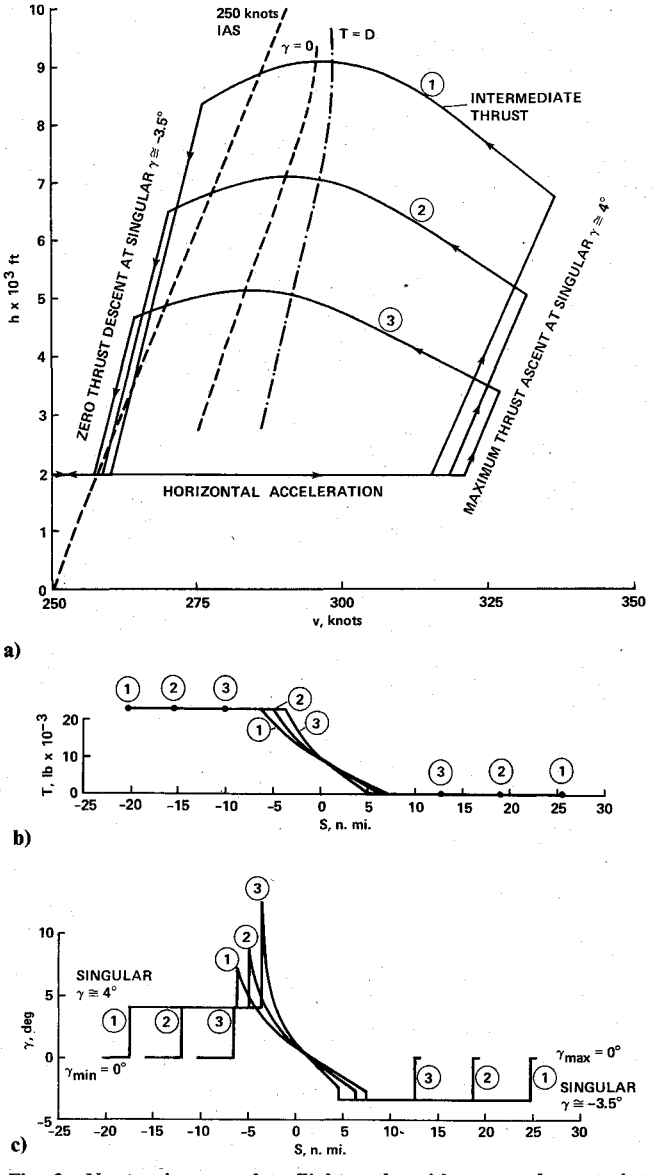

Fig. 2 Nonturning complete flight paths without speed constraint and with forced horizontal turns: a) v-h profiles; b) thrust vs distance; c) flight-path angle vs distance.

turns of the climb-outs and descents, respectively. This, of course, is not optimal; and optimal formulation would require a time- and state-dependent constraint on γ, which would be exceedingly unprofitable to implement since, we estimate, it would make a negligible difference in fuel consumption. We refer to the resulting flight-paths as having *forced horizontal turns*. Climb-outs with forced horizontal turns required approximately 20 lb extra fuel, representing about a 2% increase for the climb to 10,000 ft, independent of the heading change. This increase is due to the loss of the extra acceleration afforded by the $\gamma=\gamma_{min}=-4$ deg initial dip.

We conclude by noting that the speeds at $h=10{,}000$ ft, on the singular arcs that end the climb-out and start the descent, match the corresponding speeds on the v-h profile for a medium-range, airport-to-airport nonturning flight path, computed for the same aircraft in Ref. 1.

VIII. Results: Complete Three-Dimensional Flight Paths

Figure 2a shows v-h profiles for nonturning flight paths with no speed constraint. These are of the forced horizontal type to avoid dips below 2000 ft. Thus, γ is $0\le\gamma\le_{max}=5$ deg and $\gamma_{min}=-4\le\gamma\le 0$ deg at the beginning and at the end of the paths, respectively; for $h>2000$ ft, γ is singular. The coordinate S in Figs. 2b and 2c denotes horizontal path length and $S=0$ corresponds to the start of computation at the point on the flight paths where thrust is equal to drag. The spike-like discontinuities in singular γ seen in Fig. 2c are due to the discontinuities in $\dot{T}$ shown in Fig. 2b [which appears in Eq. (28) for singular γ] at junctions of intermediate T and bounded T (at the corners in Fig. 2a). These spikes exceed the bound $\gamma_{max}=5$ deg and the assumption of "small" γ. To be mathematically correct, we should leave the singular arc when the bounds are exceeded. However, we ignored this for computational expediency, because it would be exceedingly difficult to return to the singular arc. The advantage in fuel use that such a flight path has over one for which $\gamma=\gamma_{max}=5$ deg is observed, was estimated (by comparison with near-optimal paths that do not exceed $\gamma_{max}=5$ deg) to be less than 0.2%.

Figure 3 shows the altitude profiles against the horizontal path length S for nonturning flight paths where altitude dips were permitted. We observe the dips below 2000 ft along $\gamma_{min} = -4$ deg and $\gamma_{max} = 5$ deg. If these bounds are set to zero as in the case of Fig. 2, the dips are replaced by a horizontal path, but otherwise the curves remain the same. The fuel gain of allowing these dips below 2000 ft is 4 lb for flight paths of equal length. We also observe the change in slope, corresponding to the spikes in singular γ in Fig. 2b, as the thrust goes from maximum to intermediate values.

Figure 4 shows the x-y plot of long, turning complete paths that reach a peak altitude of about 7000 ft; here $v(0) = 250$ knots IAS, and $v_f = 180$ knots IAS; there is no speed constraint. The turns are of the forced horizontal type, where $0 \le \gamma \le 0.01$ deg for the initial turns, and $-0.01 \le \gamma \le 0$ deg for the final turns. We observe in Fig. 4 that most of the turn is done while flying horizontally. Except for paths 3 and 4, the thrust profile is identical for all flights.[16] For paths 3 and 4, the thrust starts at zero, rapidly building up to maximum. Zero thrust causes initial deceleration, hence the velocity profiles for flight paths 3 and 4 have an initial dip enabling a tighter, fuel-saving turn, a feature already observed in Ref. 12. We remark that because of the velocity dips, there is an additional point on each of flight paths 3 and 4, at $\psi = 68.9$ and 87.3 deg, respectively, where the flight could start at $v_0 = 250$ knots IAS. The singular γ is independent of the turns; hence, the altitude profile is identical for all fights and it is the same as for nonturning paths.

Results for short flights that reach a peak altitude of about 4000 ft are shown in Ref. 16. These flights are similar to the longer ones considered here, except that the thrust does not reach the maximum value and, furthermore, there is a coupling between the turns on both ends with respect to the thrust. Also, in contrast to the longer flights, the climb is not at a nearly constant singular γ and the singular arc on the descent is very short.

IX. Cost of Observing the Speed Constraint

The cost in fuel of observing the FAA imposed speed constraint of 250 knots IAS on climb-out paths is 36 lb independent of the amount of turn. [The 36 lb cost includes flying at 10,000 ft from the speed-constraint velocity of 290.5 knots (250 knots IAS) to the higher velocity of 340 knots dictated by the singular arc at that altitude, so that for the comparison the end speeds are the same; the different x distance is accounted for by the term $CV\cos\psi$.] From this 10,000 ft, 340 knot point we assume that the flight continues optimally with further climb and acceleration as per Ref. 1. For the case of a 200 n.mi. flight path the 36 lb represent 0.7% of the total fuel. For descents the cost of observing the speed constraint is only about 1 lb. The cost for nonturning complete speed limited flight paths is about 3.7% over the nonspeed-limited flight paths, for example, 50 lb of fuel on a 52 n.mi. long path. Observing the speed constraint somewhat alters the flight paths, but the comparison is with matching end points.

X. Fuel Comparison with Nonoptimal Flight Paths

How much fuel is saved by flying optimal paths? To get an idea, we compared three turning climb-out procedures with optimal ones having forced horizontal turns. The v-h profiles for these three procedures are shown in Fig. 5. All turns are with maximum bank angle; following the turn, a straight line path as projected in the horizontal plane was followed until the speed for the approximate (i.e., average constant) singular arc is reached. The flight paths are with $T = T_{max}$ throughout and are matched in h, ψ, and v at their ends (the different ranges are corrected for by the term $Cv\cos\psi$). The results show that, for turns of 0-180 deg, respectively, procedure (a) requires 10-30% more fuel than the optimal one and procedure (b) is 3-5% worse than optimal. Procedure (c), which best approximates the optimal one, consumes less than 2% more fuel than optimal for all heading changes. Thus, it is clear that the most important fuel-saving feature of the optimal climb-out is the horizontal turn and acceleration; a procedure that calls for simultaneous turn, acceleration, and climb, such as procedure (a), is fuel wasteful. Similar conclusions hold for the descent which, as already noted, is far less fuel-critical than the climb-out.[16]

We also compared the fuel consumption for complete nonturning optimal flight paths that started and ended at $h = 2000$ ft and $v_I = 250$ knots IAS with three nonoptimal procedures, as a function of horizontal flight-path length. Compared to the optimal, flying at constant altitude ($h = 2000$ ft) and at constant speed ($V_I = 250$ knots) takes between 5% and 10% more fuel for path lengths of 20-45 n.mi. Flying at constant altitude ($h = 2000$ ft) but using the near-optimal acceleration and deceleration algorithm described in Ref. 21, which ap-

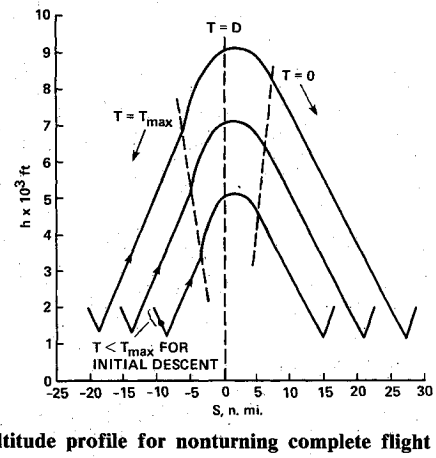

Fig. 3 Altitude profile for nonturning complete flight paths with altitude dips.

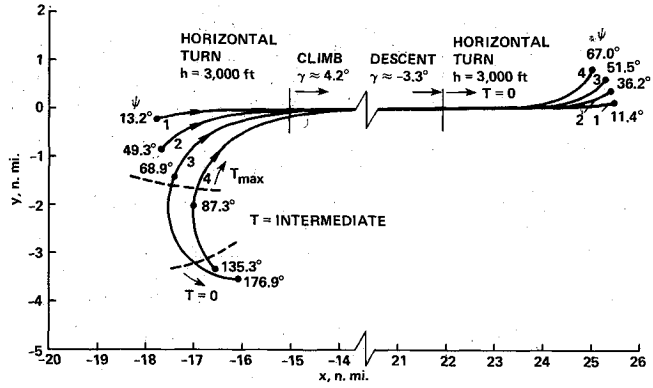

Fig. 4 x-y plot of long turning complete flight paths.

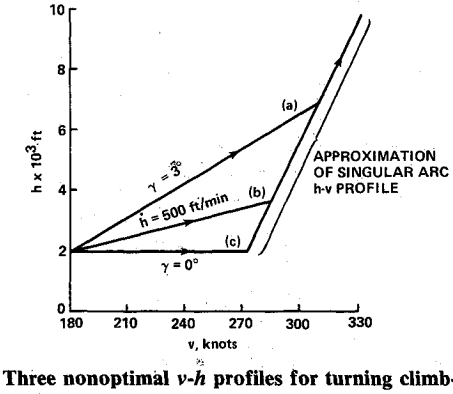

Fig. 5 Three nonoptimal v-h profiles for turning climb-out.

proximates the optimal nonturning flight paths of Ref. 12 and which solves the two-point boundary value problem, results in the use of between 1 and 5% more fuel than the optimal. The results for a near-optimal algorithm described in Ref. 15, which besides solving the two-point boundary value problem also includes climb to and descent from a higher altitude, are within 0.2% of optimal and, in contrast to the other two procedures, the approximation improves with path length. The algorithm of Ref. 16 produces similarly good approximations for turning complete flight paths.

XI. Conclusions

This paper presents the computation of minimum-fuel nonturning and turning flight paths for climb-outs from 2000 to 10,000 ft for long-range flights (greater than 50 n.mi.), and for complete flight paths of lengths between 5 and 50 n.mi.

An important result is that the optimal flight paths have turns with little altitude change, which are practically decoupled from the climb and descent portions. The latter are at almost constant flight-path angles. For the short flight paths considered, no steady-state cruise exists where the flight path angle is zero and the thrust equals the drag. Instead, there exists a variable-thrust, variable-angle segment that connects the climb-out and descent portions of the flight paths. These features facilitate near-optimal algorithms; one such algorithm provided very good approximation. Turning horizontally and then climbing when the proper speed is reached —rather than turning and climbing simultaneously—is the principal fuel-saving feature of the optimal flight paths. Allowing speeds on climb to freely exceed the FAA-imposed 250 knots IAS limit affords fuel savings of 36 lb per climb-out.

Are the flight paths we computed indeed optimal? This is a pertinent question because the extremals satisfy only necessary conditions and Darboux points (beyond which the extremal ceases to be globally optimal) may indeed appear. We believe, however, that by limiting turns to less than 180 deg, we avoided Darboux points (unlike for conjugate points, there exists no test for Darboux points).

The fuel savings afforded by flying optimal flight paths in the terminal area are, of course, small in relation to the fuel expenditure of complete long-distance airport-to-airport flights. However, the cumulative saving is significant. With the present trend toward automation of air traffic control, we feel it is economically worthwhile and definitely feasible to incorporate fuel-saving, near-optimal algorithms into future onboard flight-path management systems.

Appendix A: Fuel Flow and Drag

The following numerical values are least-square fits to tabular data for the fuel flow rate F and drag D for a Boeing 727 below 10,000 ft altitude.

$$F=[c_1(1+c_2h)+c_3(1+c_4h)v]+[c_5(1+c_6h)+c_7(1+c_8h)v]T+[c_9(1+c_{10}h)+c_{11}(1+c_{12}h)v]T^2$$
$$=C_0+C_1T+C_2T^2$$

$c_1=0.47537$ $\quad c_7=0.15898\times10^{-6}$

$c_2=-0.24360\times10^{-4}$ $\quad c_8=-0.12439\times10^{-4}$

$c_3=0.17702\times10^{-2}$ $\quad c_9=0.91747\times10^{-9}$

$c_4=-0.28995\times10^{-4}$ $\quad c_{10}=0.79644\times10^{-4}$

$c_5=0.10823\times10^{-3}$ $\quad c_{11}=-0.85521\times10^{-12}$

$c_6=-0.80509\times10^{-5}$ $\quad c_{12}=-0.45624\times10^{-4}$

$$D=k_1(1+k_2h)+k_3(1+k_4h)v^2+k_5(1+k_6h)/v^2+[k_1(1+k_2h)/2+k_5(1+k_6h)/v^2]u^2=D_1+D_2u^2$$

$k_1=-0.4078\times10^4$ $\quad k_4=-0.2005\times10^{-4}$

$k_2=0.2429\times10^{-4}$ $\quad k_5=0.3830\times10^9$

$k_3=0.1146$ $\quad k_6=0.4227\times10^{-4}$

Appendix B: Computation of Singular γ

The conditions $0=\dot{H}=H_\gamma=\dot{H}_\gamma$ give

$$0=-F_hv+\lambda_v[D_hv+g(T-D)/v-gD_v]g/W+g(F_v+\lambda_x\cos\psi+\lambda_y\sin\psi+\lambda_\psi gu/v^2) \tag{B1}$$

We assumed here that the speed constraint is inactive, hence $\eta=0$. Further time differentiation yields

$$(\ddot{H}_\gamma)=\frac{\partial\dot{H}_\gamma}{\partial t}$$

$$0=\frac{\partial}{\partial t}\left\{-F_hv+\lambda_v[D_hv+g(T-D)/v-gD_v]g/W+g(F_v+\lambda_x\cos\psi+\lambda_y\sin\psi+\lambda_\psi gu/v^2)\right\}$$
$$=A_H^*\dot{v}+B_H^*\dot{h}+C_H^*\dot{\psi}+D_H^*\dot{\lambda}_v+E_H\dot{\lambda}_\psi \tag{B2}$$

where the coefficients have the following values

$$A_H=-F_h+gD_h\lambda_v/W-g^2\lambda_v(T-D)/(Wv^2)-2g^2\lambda_\psi u/v^3-g^2\lambda_vD_v/(Wv)+Q_H[1-k_1(1+k_2h)/D_2]/v-vF_{vh}+2gk_3k_4v^2\lambda_v/W-2gk_5k_6(1+u^2)\lambda_v/(Wv^2)-2g^2k_3(1+k_4h)\lambda_v/W-6\lambda_vg^2k_5(1+k_6h)(1+u^2)/(v^4W)$$

$$B_H=-g^2\lambda_vD_h/(Wv)-Q_HD_{2_h}/D_2+gF_{vh}-2g^2k_3k_4v\lambda_v/W+2g^2k_5k_6(1+u^2)\lambda_v/(Wv^3) \tag{B3}$$

$$D_H=g[D_hv+g(T-D)/v-gD_v]/W-Q_H/\lambda_v$$

$$E_H=g^2u/v^2+Q_H/\lambda_\psi$$

$$Q_H=[g^2\lambda_\psi/v^2-g^2\lambda_vD_u/(Wv)+(k_1k_2v+2k_5k_6/v)g\lambda_vu/W+4g^2k_5(1+k_6h)u\lambda_v/(Wv^3)]u,\quad |u|<u_m$$

$$Q_H=0,\quad |u|=u_m$$

$$A_H^*=A_H+g^2\lambda_v\tau_v/(Wv)+\tau_v(gF_{vT}-vF_{hT}) \quad 0<T<T_{\max}$$
$$=A_H \quad T\equiv0,\ T\equiv T_{\max}$$

$$B_H^*=B_H+g^2\lambda_v\tau_h/(Wv)+\tau_h(-vF_{hT}+gF_{vT}) \quad 0<T<T_{\max}$$
$$=B_H \quad T\equiv0,\ T\equiv T_{\max} \tag{B4}$$

$$C_H^* = -g(\lambda_x \sin\psi - \lambda_y \cos\psi)$$

$$D_H^* = D_H + \tau_{\lambda_v}[g^2\lambda_v/(Wv) - F_{hT}v + gF_{vT}] \quad 0 < T < T_{\max}$$

$$= D_H \quad T \equiv 0,\ T \triangleq T_{\max}$$

Using in Eq. (B2) the right side of Eqs. (3-5), (14), and (15) for the derivatives $\dot{v}$, $\dot{h}$, $\dot{\psi}$, $\dot{\lambda}_\psi$, and setting Eq. (B2) to zero, gives Eq. (27) whence Eq. (28) is

$$\gamma = [A_H^* g(T-D)W - C_H^* g u/v + D_H^*(-F_v - \lambda_x \cos\psi - \lambda_y \sin\psi - \lambda_\psi g u/v^2 + \lambda_v g D_v/W) + E_H(\lambda_x v \sin\psi - \lambda_y v \cos\psi)]/(A_H^* g - B_H^* v + D_H^* \lambda_h) \quad \text{(B5)}$$

Acknowledgments

The authors wish to thank Dr. Heinz Erzberger for his continuing support in this project. A special thanks goes to Dr. Joseph Shinar, who emphasized the importance of the singular arc in the solution of this problem, and to Dr. G. Allen Smith for his careful editing of the original report.

References

[1]Erzberger, H., and Lee, H., "Constrained Optimum Trajectories with Specified Range," *Journal of Guidance and Control,* Vol. 13, Jan.-Feb. 1980, pp. 78-85.

[2]Burrows, J.W., "Fuel-Optimal Trajectory Computation," *Journal of Aircraft,* Vol. 19, April 1982, pp. 324-329.

[3]Burrows, J.W., "Fuel-Optimal Aircraft Trajectories with Fixed Arrival Times," *Journal of Guidance, Control, and Dynamics,* Vol. 16, Jan.-Feb. 1983, p. 14-19.

[4]Chakravarty, A., "4th Fuel-Optimal Guidance in the Presence of Winds," AIAA Paper 83-2242, Aug. 1983.

[5]Gordon, C.N., "Flight Software for Optimal Trajectories of Transport Aircraft," AIAA Paper 83-2241, Aug. 1983.

[6]Ralaitsizafy, A.M.C., "Sur les Equations Generales d'Optimization du Vol des Avions de Transport," *Revue Roumaine des Sciences Techniqus, Ser. de Mechanique Appliquee,* Vol. 28, July-Aug. 1983, pp. 413-425.

[7]Hedrick, J.K. and Bryson, A.E. Jr., "Three-Dimensional Minimum-Time Turns for a Supersonic Aircraft," *Journal of Aircraft,* Vol. 9, Feb. 1972, pp. 115-121.

[8]Hedrick, J.K. and Bryson, A.E., Jr., "Three-Dimensional, Minimum Fuel Turns for a Supersonic Aircraft," *Journal of Aircraft,* Vol. 9, March 1972, pp. 223-229.

[9]Humphreys, R.P., Hennig, G.R., Bolding, W.A., and Helgeson, L.A., "Optimal 3-Dimensional Minimum Time Turns for an Aircraft," *Journal of the Astronautical Sciences,* Vol. 20, No. 2, Sept.-Oct. 1972, pp. 88-112.

[10]Parson, M.G., Bryson, A.E. Jr., and Hoffman, W.C., "Long-Range Energy-State Maneuvers for Minimum Time to Specified Terminal Conditions," *Journal of Optimization Theory and Applications,* Vol. 17, Nos. 5-6, Dec. 1974, pp. 447-463.

[11]Neuman, F. and Kreindler, E., "Optimal Turning Climb-Out and Descent of Commercial Jet Aircraft," SAE Paper 821468, Society of Automotive Engineers, Warrendale, Pa., Oct. 1982.

[12]Kreindler, E. and Neuman, F., "Minimum Fuel Horizontal Flightpaths in the Terminal Area," *Journal of Guidance, Control, and Dynamics,* Vol. 5, Sept.-Oct. 1982, pp. 490-497.

[13]Kreindler E. and Neuman, F., "Darboux Points in Minimum-Fuel Aircraft Landing Problems," *Preprint Volume, Joint Automatic Control Conference,* University of Virginia, Chalottesville, Va., June 17-19, 1981.

[14]Kriendler, E. and Neuman, F., "Global Optimality of Extremals: An Example," *Journal of Optimization Theory and Applications,* Vol. 36, April 1982, pp. 521-534.

[15]Schultz, R.L. and Zagalsky, N.R., "Aircraft Performance Optimization," *Journal of Aircraft,* Vol. 9, Feb. 1972, pp. 108-114.

[16]Neuman, F. and Kreindler, E., "Minimum Fuel 3-Dimensional Flightpath Guidance of Transport Jets," NASA TP-2326, Sept. 1984.

[17]Leitmann, G., *The Calculus of Variations and Optimal Control,* Plenum Press, New York, 1981.

[18]Jacobson, D.H., Lele, M.M., and Speyer, J.L., "Necessary Conditions of Optimality for Control Problems with State-Variable Inequality Constraints," *Journal of Mathematical Analysis and Applications,* Vol. 35, 1971, pp. 255-284.

[19]Bell, D.J., and Jacobson, D.H., *Singular Optimal Control Problems,* Academic Press, New York, 1975.

[20]Maurer, H., "On Optimal Control Problems with Bounded State Variables and Control Appearing Linearly," *SIAM Journal of Control and Optimization,* Vol. 15, No. 3, May 1977, pp. 345-362.

[21]Neuman, F. and Erzberger, H., "Algorithm for Fuel Conservative Horizontal Capture Trajectories," NASA TM-81334, 1981.